Learning Multiple Radiation Source Distribution Models using Gaussian Processes

David De Schepper[1,2], Mattias Simons[3], Wouter Schroeyers[3], Karel Kellens[1,2] and Eric Demeester[1,2]

***Abstract*—Over the past years, automated, robotic radiation source localisation has become of emerging interest due to a variety of reasons, e.g. disaster response, homeland security, or dismantling and decommissioning of nuclear contaminated areas. Nowadays, to perform in-the-field measurements, radiation protection officers and safety personnel are tasked with characterising an environment before a nuclear contaminated area can enter the final phase of the dismantling and decommissioning process. This involves some severe drawbacks such as the absence of any a priori information on the potentially contaminated area. Besides the potential health risks involved, this preliminary task is very time-consuming and prone to errors concerning the taken measurements and the post-processing of the obtained measurements. To further automate this task, this paper presents an approach to build a radiation model of the environment based on measurements collected by a robotic arm during in-situ laboratory tests. The task of estimating the radiation distribution in an environment is modeled as a regression problem, where the framework of Gaussian Processes is adopted. The experiments conducted in an in-situ laboratory environment demonstrate that the approach is feasible to model the radiation distribution caused by multiple radiation point sources, for both static measurements, where a robot stops moving to sample a measurement, and dynamic measurements, where a robot executes measurements in a continuous manner.**

***Index Terms*—Robotics for nuclear power plants; Radiological mapping; Gaussian Processes; Field robotics; Robotic exploration**

I. Introduction

Over the past decades, a substantial amount of research has been conducted in the field of localising nuclear radiation sources, often abbreviated by hot spots. Localising these hot spots has become of emerging interest for a variety of purposes, e.g. homeland security, leakage detection, and dismantling and decommissioning (D&D) of nuclear power plants. Nowadays, to start with the activities towards the latter, safety personnel are sent out in the field to characterise the environment by taking ambient dose rate measurements, atmospheric contamination, and surface contamination measurements. This task, however, contains various risks. The physical state of the personnel needs to be continuously monitored to prevent potential health damage. Moreover, this task is very time-consuming, and in practice, these measurements can vary from a few minutes up to a few hours, depending on the geometric properties of the environment. Furthermore, the uncertainties of these measurements cannot be neglected. Due to these disadvantages, a high demand towards fully autonomous robots can be observed. The task of such a robot is threefold. Firstly, the robot has to gather geometric information of the environment. In robotics, this task is performed by simultaneous localisation and map building algorithms. Based on measurements received by, and actions taken by the robot, the map and the location of the robot in that particular map is sequentially updated. Secondly, an autonomous robot has to characterise the identified nuclear radiation sources by making use of spectral measurements, captured by (a) radiation detection device(s), which can take up a few minutes to a few hours. Finally, the robot has to decontaminate the identified sources. Motivated by the challenges as described above, in this paper we present a supervised regression approach based on the Gaussian Processes framework to model the radiation distribution stemming from multiple unknown radiological point sources in the environment. Based on a dataset collected during in-situ laboratory experiments, the parameters from the GP model are learned. The approach shows that the problem of multiple radiation source localisation can be tackled both in the case of performing static measurements defined by a grid of points, and by executing a continuous movement without the need to stop to sample a measurement. The remainder of the paper is organised as follows. Section II initiates with related work concerning robotics in nuclear environments, robotic tools to localise radiation sources, and the usage of the Gaussian Processes framework in robotics. Section III briefly delineates the working principle of the used sensor to measure levels of radiation in an environment. Section IV discusses our overall approach to the multiple radiation source distribution mapping problem. Section V illustrates the

[1] KU Leuven, Department of Mechanical Engineering, Campus Diepenbeek, ACRO Research Group, Wetenschapspark 27, 3590 Diepenbeek, Belgium.

[2] Flanders Make @ KU Leuven, Belgium

[3] Hasselt University, Faculty of Engineering Technology, CMK, Nuclear Technology Centre, Agoralaan, gebouw H, 3590 Diepenbeek, Belgium.

Corresponding author: david.deschepper@kuleuven.be

The authors gratefully acknowledge KU Leuven, Diepenbeek Campus, for granting a FLOF mandate, facilitating this research. This work was also supported by the Fund for Scientific Research Flanders (Fonds Wetenschappelijk Onderzoek (FWO)) scholarship nr 1SA2621N.

results of the presented approach in an in-situ environment performing static and dynamic measurements. Finally, conclusions are drawn in section VI, and some tracks for future work are discussed.

II. Related work

Research towards (semi-)autonomous localisation of radiation point sources has been focusing on either the electro-mechanical aspects of designing robotic systems that can be adopted in radiological environments, or on the development of software algorithms to solve the problem of identifying contaminations in the environment. The latter is known as radiation source localisation or radiation mapping. In literature, multiple approaches for robotic devices are presented. In [1], an approach is described for the design and development of a mobile, autonomous, radiological-monitoring robot called CARMA. It was the first proof-of-concept robot that was designed to be deployed into an active nuclear site in Europe. In the proof-of-concept experiments, the robot showed it was capable of identifying and localising α radiation acquired from a single point source at the Sellafield nuclear site. In previous work [2], a ground-based mobile manipulator proof-of-concept robot is developed suited for radiological monitoring purposes. Experiments show that a wall can be automatically scanned and characterised. Next to ground-based mobile robots, research has also been carried out towards semi-autonomous aerial vehicles [3]–[5], and even remote operated vehicles for underwater exploration and monitoring which has lead to several tests at the Fukushima Daiichi plant [6]–[9]. Additionally, research has concentrated on developing techniques to solve the problem of radiation source localisation in, often cluttered, nuclear environments. This is a very challenging problem due to (i) the non-linearity of radiation intensity propagation. This follows the inverse square law of intensity propagation; (ii) unknown a priori information of the environment. The amount of sources, their respective activities, and the background intensity are often unknown, but very important parameters in order to solve the localisation problem; (iii) the relative high cost of implementing radiation detectors. However, in more recent years several approaches have been implemented towards nuclear radiation source localisation where the uncertainty of measuring radiation is taken into account. In [10], the potential of applying Bayesian techniques for radiological source detection and localisation is explored. Baidoo-Williams et al. [11] explored nuclear source localisation and tracking through maximum likelihood techniques. Their approach was applied on the case of a stationary nuclear source and a moving target with a radiological measurement tool. The approach was, however, only feasible for perfect measurements, i.e. uncertainties in measurements are not taken into account. The approach worked well with one radiation source, which was a priori known. The authors in [12] presented a probabilistic approach towards multiple nuclear sources localisation. The foundation of this approach lies in the fact that multiple sources can be estimated using multiple sensors, or a network of sensors distributed in the area to be measured. Though this approach is robustly designed, a network of distributed sensors is needed to make it work. In many applications, e.g. exploration of unknown terrain before dismantling and decommissioning, a network of sensors cannot be installed a priori. Gao et al. [13] extended the approach of Chin et al. to just one radiation detector, mounted on the tool center point (TCP) of a mobile manipulator. The approach of [14] adopted a range and bearing sensor using a Compton Gamma camera to localise a single radiation source in a 3D environment. As a measurement model, the authors adopted a range and bearing based model, containing an intensity, and the elevation and azimuth angle of the estimated radiation source. Mascarich et al. [15] used a mobile robot, mounted with three radiation sensors to estimate the distributed radiation in a 3D environment. In order to actively control a mobile robot, with three, under 120 degrees radially mounted, Thallium-doped Cesium Iodide (CsI(TI)) radiological sensors combined with Silicon Photomultipliers (SiPm) and a LIDAR sensor, an informative path planning algorithm was adopted. This formation allows the algorithm to compute the 2D field gradient immediately. The field gradient is calculated as a weighted difference over two measuring times from the corresponding radiation sensor. Gaussian Processes (GPs) have been used in a variety of robot applications, going from WiFi-based localisation [16], learning observation models for laser range finders [17] and user models for semi-autonomous wheelchair navigation [18], to mapping high concentrations of gas [19], [20]. The framework has also been used in order to map elevated levels of radiation coming from a single radiation source [21], [22]. In [21], a GP approach was examined for the purpose of intensity mapping in complex radiation fields. The built GP model of a single radiation source was used together with a Monte Carlo N-Particle based case study to illustrate the potential of integrating the GP model for inter- and extrapolating predictions of the model. The authors however propose the integration of multiple sensors to perform the mapping of an environment. The authors of [22] used a Gaussian Process Regression technique to create a radiation map based on sparse and noisy measurements of radiation. Based on real experiments at a nuclear facility, the approach was able to recreate a model of the environment where a single source of radiation was successfully reconstructed.

III. Working principle of the used radiation sensor

A Cadmium-Zinc-Telluride (CdZnTe, CZT) sensing device, which is adopted in this work, works according to the following principle. X-ray or gamma (γ) radiation emits photons ranging from low-energetic photons to photons containing high energy. Radioactive materials emit, depending on the type of radionuclide, α, β, or γ radiation. Sensors containing a CZT semiconductor crystal can measure γ radiation or X-ray radiation. The first interaction between γ radiation or X-ray radiation with the sensing device happens in the semiconductor crystal. Ionising radiation interacts with the detector in the CZT crystal. This absorbed ionising radiation excites electron-hole pairs in proportion to the deposited energy of the emitted photon. The amount of generated electron-hole pairs is mathematically represented using formula 1:

$$n_0 = \frac{E_0}{\epsilon} \tag{1}$$

where n_0 is the number of generated electron-hole pairs, E_0 is the deposited energy of the photon particle and ϵ is the average consumed energy to create an electron-hole pair [23]. Electrons are negatively charged, while holes are positively charged. By applying an electric field across the detector, the detector causes two currents, i.e. an electron current (i_e) and a hole current (i_h). The electron current will drift towards the anode, while the hole current will drift towards the cathode. This will introduce a charge on the electrodes Q_{ind}, which in turn will result in a current $i(t)$. This resulting charge pulse will be captured and fed into a charge sensitive pre-amplifier, which produces a voltage pulse, with the amplitude of the pulse being proportional to the incident energy of the absorbed photon. Thereafter, the output pulses from the pre-amplifier are fed into a shaping amplifier, which converts the pulse into a Gaussian shape and at the same time providing further amplification. These clean pulses can then typically be fed into a suitable counter or multi-channel analyser (MCA) which enables the characteristic spectrum for the incoming photons to be generated.

IV. Radiation modeling described as a Gaussian Process

A. Gaussian Processes

A Gaussian Process, often abbreviated by $\mathcal{GP}$, is a collection of random variables, any finite number of which have a joint Gaussian distribution [24]. A Gaussian Process defines a distribution of functions $f(\mathbf{x}) : \chi \rightarrow \mathbb{R}$ in function space. Function values ($f(\mathbf{x})$) form this collection of random variables with joint Gaussian distribution of every finite subset of them. The Gaussian Process is completely defined by its mean and covariance function:

$$\begin{aligned} f(\mathbf{x}) &\sim \mathcal{GP}(m(\mathbf{x}), k(\mathbf{x}, \mathbf{x}')) \\ m(\mathbf{x}) &= \mathbb{E}[f(\mathbf{x})] \\ k(\mathbf{x}, \mathbf{x}') &= \mathbb{E}[(f(\mathbf{x}) - m(\mathbf{x})(f(\mathbf{x}') - m(\mathbf{x}'))] \end{aligned} \tag{2}$$

Gaussian Processes provide a Bayesian framework for *regression*, where learning is specified in terms of Gaussian probability density functions. The mean function, $m(\mathbf{x})$, can be set to zero provided that all training values are normalised to zero mean before estimating the Gaussian Process. The covariance function, or kernel function $k(\mathbf{x}, \mathbf{x}')$, encodes all the properties about the unknown function, $f(\mathbf{x})$, to be learned. In order to use the $\mathcal{GP}$ framework in a correct way, only positive semi-definite covariance functions are valid. Given a set of training data $\mathcal{D} = \{(\mathbf{x}_i, y_i)\}_{i=1}^n$, where $\mathbf{x}_i \in \mathbb{R}^d$ are the input data and $y_i \in \mathbb{R}$ are the target data. The goal of the regression framework is to predict target values $y_* \in \mathbb{R}$ at a new input point $\mathbf{x}_*$. Let $\mathbf{X} = [\mathbf{x}_1; \ldots; \mathbf{x}_n]^T$ be the $n \times d$ matrix of the input data and $\mathbf{X}_*$ be defined analogously for multiple test data points. In the $\mathcal{GP}$ model, any finite set of samples is jointly Gaussian distributed. The joint distribution of the observed target values and the function values at the noisy test locations, samples from the prior of a $\mathcal{GP}$ model, can be written as

$$\begin{bmatrix} \mathbf{y} \\ \mathbf{f}(\mathbf{X}_*) \end{bmatrix} \sim \mathcal{N}\left(\mathbf{0}, \begin{bmatrix} k(\mathbf{X}, \mathbf{X}) + \sigma_n^2 \mathbf{I} & k(\mathbf{X}, \mathbf{X}_*) \\ k(\mathbf{X}_*, \mathbf{X}) & k(\mathbf{X}_*, \mathbf{X}_*) \end{bmatrix}\right) \tag{3}$$

where $k(\mathbf{X}, \mathbf{X})$ refers to the covariance matrix (or kernel function) built by evaluating the covariance function $k(.,.)$ for all pairs of all row vectors $\langle \mathbf{x}_i, \mathbf{x}_j \rangle$ of $\mathbf{X}$. To make predictions of $\mathbf{X}_*$, we take the joint conditional Gaussian prior distribution on the observations, which results in the predictive mean, and predictive covariance function:

$$\mathbf{f}_* | \mathbf{X}, \mathbf{y}, \mathbf{X}_* \sim \mathcal{N}\left(\bar{\mathbf{f}}(\mathbf{X}_*), \mathbb{V}\left[\mathbf{f}(\mathbf{X}_*)\right]\right) \tag{4}$$

where

$$\begin{aligned} \bar{f}(\mathbf{X}_*) \triangleq \mathbb{E}\left[\mathbf{f}(\mathbf{X}_*)\right] = \\ k(\mathbf{X}_*, \mathbf{X}) \cdot \left[k(\mathbf{X}, \mathbf{X}) + \sigma_n^2 \mathbf{I}\right]^{-1} \mathbf{y} \end{aligned} \tag{5}$$

$$\begin{aligned} \mathbb{V}\left[\mathbf{f}(\mathbf{X}_*)\right] = k(\mathbf{X}_*, \mathbf{X}_*) - k(\mathbf{X}_*, \mathbf{X}) \\ \times \left[k(\mathbf{X}, \mathbf{X}) + \sigma_n^2 \mathbf{I}\right]^{-1} k(\mathbf{X}, \mathbf{X}_*) \end{aligned} \tag{6}$$

More information on the derivation of $\mathcal{GP}$ model priors and predictions can be found in [24].

B. Learning the radiation model from data

Given a training set $\mathcal{D} = \{(\mathbf{x}_j, y_j)\}_{j=1}^n$ of radiation intensity measurements y_j sampled at the corresponding sensing locations $\mathbf{x}_j$, the task is to learn the $\mathcal{GP}$ model. The training set is visually represented by figure 1. Figure 1a represents the observed amount of sampled radiation information with respect to the total

time of data captation. Figure 1b depicts the training set as a stem plot, where the x and y position shows the two-dimensional tool pose of the robot used to capture the dataset, and the Z axis shows the amount of concentration of ionising radiation captured by the radiological detector. Figure 2 in turn illustrates the used robotic arm for in-situ data collection. A first step towards the learning of a $\mathcal{GP}$ model lies in the choice of the appropriate covariance function. The intensity of radiation decreases quadratic with the distance. The Radial Basis Function (RBF) and the Matérn kernels are therefore preferable as they return to minimum value as distances to a test point increases. This gives a better representation of the nature of point source radiation intensity [22]. In this work, the Matérn class of covariance functions is used:

$$k_{\nu=3/2}(r) = \left(1 + \frac{\sqrt{3}r}{l}\right) \exp\left(-\frac{\sqrt{3}r}{l}\right) \tag{7}$$

$$k_{\nu=5/2}(r) = \left(1 + \frac{\sqrt{5}r}{l} + \frac{5r^2}{3l^2}\right) \exp\left(-\frac{\sqrt{5}r}{l}\right) \tag{8}$$

in particular, the covariance function expressed in equation 7, where l denotes the characteristic length-scale, and r the input distance. Based on the input training data and the chosen covariance function, with arbitrary chosen hyperparameters, a prior $\mathcal{GP}$ model can be calculated. This gives us the $\mathcal{GP}$ prior. To fully learn the $\mathcal{GP}$ model, i.e. the posterior distribution function, the hyperparameters should be estimated. These are estimated by maximising the marginal likelihood. For this, the open-source implementation of Gaussian Processes in Python, `GPy`, was used [25].

V. Experimental results

In this work, two different types of experiments were conducted in which data is collected. The first one consists of a full *static* dataset collection, where the robotic arm explicitly stops at discrete positions in the environment, followed by a sampling measurement of the radiation detector during an amount of time. The second type consists of a *dynamic* dataset collection, where the robotic arm executes a trajectory, and where the radiation sensor samples data at a fixed frequency. Figure 2 shows the robotic setup used for static and dynamic data collection. Figure 3 depicts the in-situ measurement setup, consisting of a Kinova Jaco robotic arm with six degrees of freedom, a Kromek CZT sensor mounted at the end effector of the Kinova robotic arm, and the used radiological point sources. An overview of the different radionuclides used in this work can be found in table I, together with their activities at calibration time, and the actual activities at data collection time.

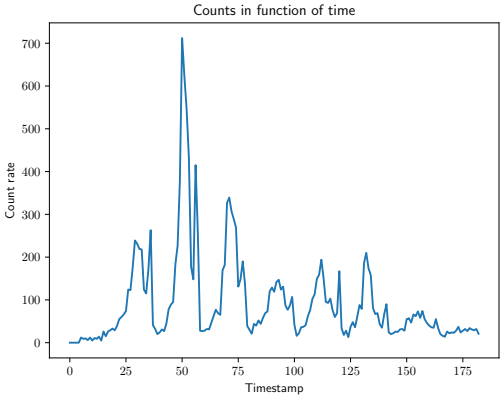

(a)

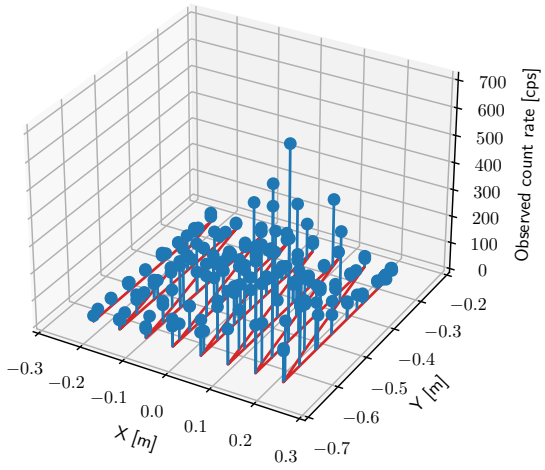

(b)

Fig. 1: Count rate information serving as input dataset. Figure 1a depicts the received count rate (total received counts per second) in function of time during the in-situ laboratory test. Figure 1b illustrates the same concentration of radiation at sampled (x, y) positions acquired by a robot arm. The distribution consists of a solid background count rate and several peaks, indicating zones of elevated radiation.

Isotope	Activity [kBq]	Half time [years]	Actual activity [kBq]
^{241}Am	418,10	458,00	391,99
^{137}Cs	412,60	30,00	154,19
^{60}Co	405,50	5,26	1,48
^{152}Eu	1651,00	13,55	1.536,86
^{137}Cs	333,00	30,00	227,97
^{57}Co	685,00	0,74	173,02

TABLE I: Overview of the different radionuclides together with their properties used during the in-situ dataset collection with the robotic arm.

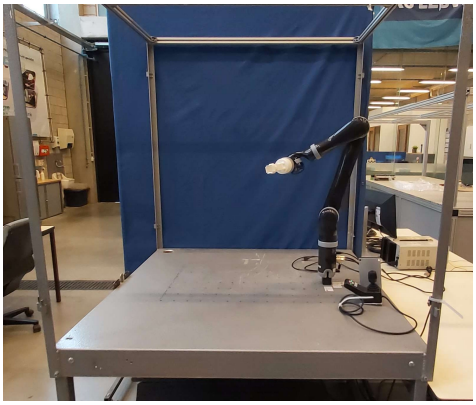

Fig. 2: A Kinova Jaco robotic arm with six degrees of freedom setup is used together with an radiological gamma ray detector spectrometer from Kromek to collect the datasets in an in-situ laboratory environment.

A. Static measurements

In the first type of experiment, the robot is tasked to perform data collection in a plane. In this *static* experiment setup, a grid of pre-defined points in the XY plane of the robot is scanned. At these points, the robot holds his trajectory execution, and waits until the Kromek device, mounted at the end effector of the robot, has sampled a measurement at this particular position. The robot is being controlled using the `C++` API at a frequency of $250Hz$, while the Kromek samples a measurement during $1s$. The vertical offset between the end effector of the robotic arm and the surface of the workbench is $0.1m$. The collected data is stored in dataset and is used in an offline phase to perform the $\mathcal{GP}$ regression with the `GPy` library. Figure 4 shows the output of the $\mathcal{GP}$ regression based on the input training set $\mathcal{D}(x, y)$, as shown in the stem plot of figure 1. Figure 4a depicts the mean function of the $\mathcal{GP}$ posterior visualised as a heatmap in a two-dimensional manner. Elevated values of radiation intensity are shown in red colors. Blue colors indicate lower radiation intensities. Together with the $\mathcal{GP}$ model, the ground truth positions of the used sources ($^{241}\mathrm{Am}$, $^{60}\mathrm{Co}$, and $^{137}\mathrm{Cs}$) to collect the dataset are drawn on figure 4a. As can be seen, two of the three sources are modeled correctly by the $\mathcal{GP}$ model.

B. Dynamic measurements

In the *dynamic* type of measurements, the robot executes a trajectory, pre-defined by a set of waypoints without completely stopping at a waypoint, while the radiological sensor samples measurements at a fixed frequency. The same constraints, i.e. control frequency of the robot, sampling frequency of the Kromek sensor, and vertical offset between robot end effector and surface, are employed. Figure 5 shows the output of the $\mathcal{GP}$ regression, illustrated again by plotting the mean function as a 2D heatmap, together with the ground truth positions of the used sources during in-situ measurements. As can be seen in figures 5a and 5b, the radiation distribution is modeled correctly with one global maximum, depicting the strongest point source, and two local maxima, indicating the two point sources of lower intensity. When comparing the $\mathcal{GP}$ model from the dynamic test setup with the one learned during the static test setup, similar results are being achieved. Both models indicate the ground truth positions of the point sources very well. The model, learned during the dynamic in-situ test, seems to model the actual distribution of point sources slightly better, by modeling a local maximum of the lowest point source, as can be seen in figure 5a. To compare the two learned $\mathcal{GP}$ models, figure 6 depicts the optimised covariance functions of the $\mathcal{GP}$ posterior during static and dynamic data collection. As can be noticed, the covariance function of the static $\mathcal{GP}$ model has values of low covariance at the positions where a measurement was sampled, and higher values at the remaining parts of the environment. In contrast, the covariance of the dynamic $\mathcal{GP}$ model has low values of covariance over the entire environment, indicating that the dynamic model is relatively more certain about its predictions. The pose of the robot end effector during dynamic dataset collection and the Cartesian end effector velocities are shown in figure 7. The Cartesian velocities are calculated by applying the forward kinematic equations, given the captured joint velocities of the robotic arm, and the robot model, using the KDL library [26]. As can be seen in figure 7, a Cartesian velocity of $\pm 0.15m/s$ is achieved during the dynamic in-situ measurements. This indicates that a continuous scanning pattern has the opportunity to perform equally compared with performing a grid-based scanning pattern, and has the benefit of increasing the speed of characterising an environment and localising radiological spots of contamination.

VI. Conclusions and Future Work

This work presented an approach towards radiation mapping and point source localisation by considering the problem of modeling the radiation distribution in an environment as a regression problem. For this, the framework of Gaussian Processes was used. Based on datasets captured during in-situ laboratory measurements with a robotic arm and a radiological device, the model of the distribution of radiation intensity in an environment is learned. The experiments showed that a realistic model of the environment can be achieved. Furthermore, it was found that a dynamic measuring principle, i.e. without effectively stopping at a certain position to sample a radiological measurement, performs equally to the static alternative, and therefore offering the opportunity to increase the speed of scanning and characterising an environment, and therefore localising source of radiological contaminations. Tracks for future work concern the evaluation of time in order to scan an environment dynamically and

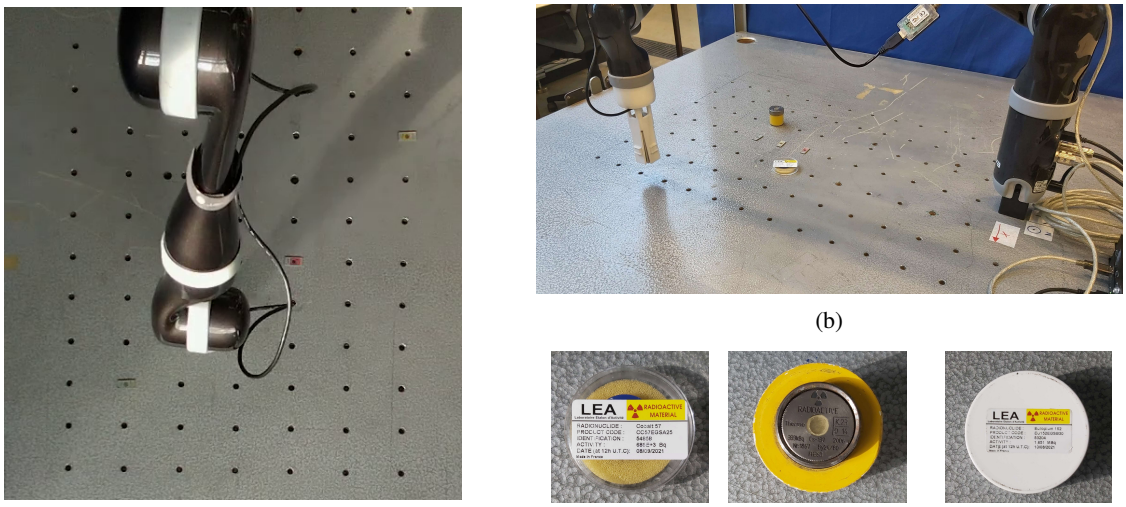

(a) (b) (c) (d) (e)

Fig. 3: Pictures while performing the in-situ laboratory experiments. Figure 3a shows the Kinova robotic arm while collecting data together with three radiological point sources lying on the surface of a workbench. Figure 3b illustrates a different dataset collection with five point sources spread over the working surface. Figures 3c, 3d, and 3e depicts the three most intense point sources (^{57}Co, ^{137}Cs, and ^{152}Eu radionuclide respectively) used in the dataset collection process.

achieving a good representation of the environment. In this work, the scanning area was rather small due to the limited work space of the robotic arm kinematics. Future work will also concern to scale up the scanning environment by using a mobile manipulator robot. Furthermore, the adopted model in this work consists of just one $\mathcal{GP}$ component. Therefore, future work will look at how well a mixture of $\mathcal{GP}$ components can model the distribution of radiation.

REFERENCES

[1] B. Bird, A. Griffiths, H. Martin, E. Codres, J. Jones, A. Stancu, B. Lennox, S. Watson, and X. Poteau, "A robot to monitor nuclear facilities: Using autonomous radiation-monitoring assistance to reduce risk and cost," *IEEE Robotics and Automation Magazine*, vol. 26, no. 1, pp. 35–43, 2019.

[2] D. De Schepper, I. Dekker, M. Simons, L. Brabants, W. Schroeyers, and E. Demeester, "Towards a semi-autonomous robot platform for the characterisation of radiological environments," in *2022 IEEE International Symposium on Safety, Security, and Rescue Robotics (SSRR)*, 2022, pp. 230–237.

[3] A. H. Zakaria, Y. M. Mustafah, J. Abdullah, N. Khair, and T. Abdullah, "Development of Autonomous Radiation Mapping Robot," *Procedia Computer Science*, vol. 105, no. April, pp. 81–86, 2017.

[4] C. Papachristos, S. Khattak, and K. Alexis, "Uncertainty-aware receding horizon exploration and mapping using aerial robots," in *2017 IEEE International Conference on Robotics and Automation (ICRA)*, May 2017, pp. 4568–4575.

[5] I. Tsitsimpelis, C. J. Taylor, B. Lennox, and M. J. Joyce, "A review of ground-based robotic systems for the characterization of nuclear environments," *Progress in Nuclear Energy*, vol. 111, no. May 2018, pp. 109–124, 2019.

[6] A. R. Jones, A. Griffiths, M. J. Joyce, B. Lennox, S. Watson, J.-i. Katakura, K. Okumura, K. Kim, M. Katoh, K. Nishimura, and K.-i. Sawada, "On the design of a remotely-deployed detection system for reactor assessment at fukushima daiichi," in *2016 IEEE Nuclear Science Symposium, Medical Imaging Conference and Room-Temperature Semiconductor Detector Workshop (NSS/MIC/RTSD)*, 2016, pp. 1–4.

[7] M. Nancekievill, A. R. Jones, M. J. Joyce, B. Lennox, S. Watson, J. Katakura, K. Okumura, S. Kamada, M. Katoh, and K. Nishimura, "Development of a radiological characterization submersible rov for use at fukushima daiichi," *IEEE Transactions on Nuclear Science*, vol. 65, no. 9, pp. 2565–2572, 2018.

[8] D. A. Duecker, N. Bauschmann, T. Hansen, E. Kreuzer, and R. Seifried, "Towards micro robot hydrobatics: Vision-based guidance, navigation, and control for agile underwater vehicles in confined environments," in *2020 IEEE/RSJ International Conference on Intelligent Robots and Systems (IROS)*, 2020, pp. 1819–1826.

[9] K. Nagatani, S. Kiribayashi, Y. Okada, K. Otake, K. Yoshida, S. Tadokoro, T. Nishimura, T. Yoshida, E. Koyanagi, M. Fukushima, and S. Kawatsuma, "Emergency response to the nuclear accident at the fukushima daiichi nuclear power plants using mobile rescue robots," *Journal of Field Robotics*, vol. 30, no. 1, pp. 44–63, 2013. [Online]. Available: https://onlinelibrary.wiley.com/doi/abs/10.1002/rob.21439

[10] M. R. Morelande and B. Ristic, "Radiological source detection and localisation using Bayesian techniques," *IEEE Transactions on Signal Processing*, vol. 57, pp. 4220–4231, 2009.

[11] H. E. Baidoo-Williams, "Maximum Likelihood Localization of Radiation Sources with unknown Source Intensity," pp. 1–5, 2016.

[12] J. C. Chin, D. K. Yau, and N. S. Rao, "Efficient and robust localization of multiple radiation sources in complex environments," *Proceedings - International Conference on Distributed Computing Systems*, pp. 780–789, 2011.

[13] W. Gao, W. Wang, H. Zhu, G. Huang, D. Wu, and Z. Du, "Robust radiation sources localization based on the peak suppressed particle filter for mixed multi-modal environments," *Sensors (Switzerland)*, vol. 18, 2018.

[14] M. S. Lee, D. Shy, W. R. Whittaker, and N. Michael, "Active Range and Bearing-based Radiation Source Localization," *IEEE International Conference on Intelligent Robots and Systems*, pp. 1389–1394, 2018.

[15] F. Mascarich, T. Wilson, C. Papachristos, and K. Alexis, "Radiation Source Localization in GPS-Denied Environments Using Aerial Robots," *Proceedings - IEEE International Conference on Robotics and Automation*, pp. 6537–6544, 2018.

[16] B. Ferris, D. Hahnel, and D. Fox, "Gaussian processes for signal strength-based location estimation," *Robotics: Science and Systems*, vol. 2, pp. 303–310, 2007.

[17] W. Burgard, O. Brock, and C. Stachniss, *Gaussian Beam*

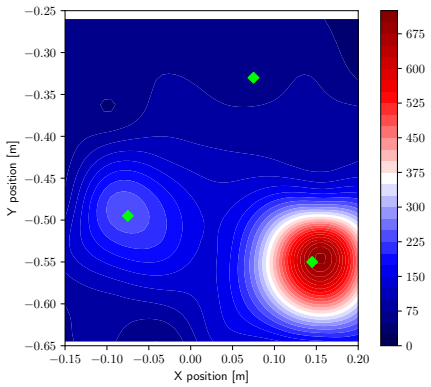

(a)

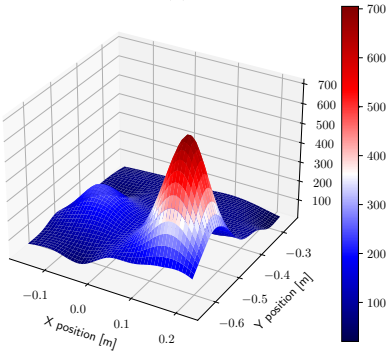

(b)

Fig. 4: Output from the Gaussian Process regression based on the input dataset $\mathcal{D}(x, y)$. Figure 4a shows a two-dimensional view of the $\mathcal{GP}$ posterior mean function after optimisation of the hyperparameters, l and σ, of the covariance function. Figure 4b depicts the same $\mathcal{GP}$ posterior mean function as in figure 4a in a three-dimensional perspective. In all the plots, a red color represents elevated values, while low(er) values are represented by a blue color. Green squares represent the actual 2D positions of the point sources in the environment.

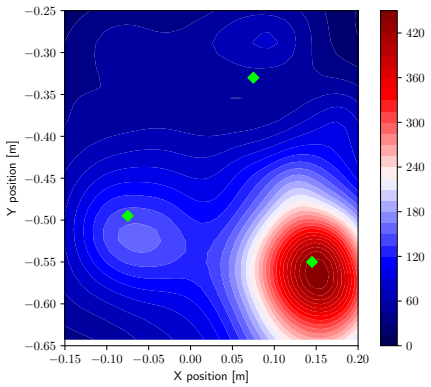

(a)

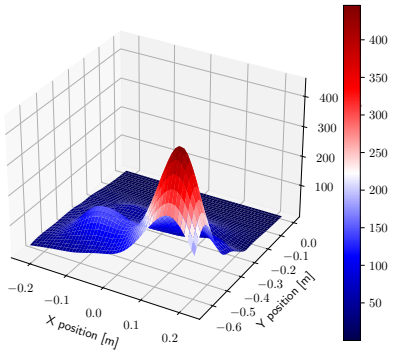

(b)

Fig. 5: Output from the Gaussian Process regression based on the input dataset captured during a dynamic collection of data. Figure 5a shows a two-dimensional view of the $\mathcal{GP}$ posterior mean function after optimisation. Figure 5b depicts the $\mathcal{GP}$ posterior mean function in a three-dimensional perspective. In all the plots, a red color represents elevated values, while low(er) values are represented by a blue color. Green squares represent the actual 2D positions of the point sources in the environment.

Processes: A Nonparametric Bayesian Measurement Model for Range Finders, 2008, pp. 137–144.

[18] A. Huntemann, E. Demeester, M. Nuttin, and H. Van Brussel, "Online user modeling with gaussian processes for bayesian plan recognition during power-wheelchair steering," in *2008 IEEE/RSJ International Conference on Intelligent Robots and Systems*, 2008, pp. 285–292.

[19] J. Burgués, V. Hernández, A. J. Lilienthal, and S. Marco, "Gas distribution mapping and source localization using a 3d grid of metal oxide semiconductor sensors," *Sensors and Actuators B: Chemical*, vol. 304, p. 127309, 2020. [Online]. Available: https://www.sciencedirect.com/science/article/pii/S0925400519315084

[20] C. Stachniss, C. Plagemann, and A. J. Lilienthal, "Learning gas distribution models using sparse gaussian process mixtures," *Autonomous robots*, vol. 26, pp. 187–202, 2009.

[21] B. A. Khuwaileh and W. A. Metwally, "Gaussian process approach for dose mapping in radiation fields," *Nuclear Engineering and Technology*, vol. 52, no. 8, pp. 1807–1816, 2020. [Online]. Available: https://www.sciencedirect.com/science/article/pii/S1738573319305935

[22] A. West, I. Tsitsimpelis, M. Licata, A. Jazbec, L. Snoj, M. J. Joyce, and B. Lennox, "Use of Gaussian process regression for radiation mapping of a nuclear reactor with a mobile robot," *Scientific Reports*, vol. 11, no. 1, pp. 1–11, 2021. [Online]. Available: https://doi.org/10.1038/s41598-021-93474-4

[23] G. R. Gilmore, *Practical Gamma-Ray Spectrometry*. John Wiley & Sons, Ltd, 2008. [Online]. Available: https://onlinelibrary.wiley.com/doi/abs/10.1002/9780470861981.fmatter

[24] C. E. Rasmussen and C. K. Williams, *Gaussian Processes for Machine Learning*. MIT Press, 2006.

[25] GPy, "GPy: A gaussian process framework in python," http://github.com/SheffieldML/GPy, since 2012.

[26] R. Smits, "KDL: Kinematics and Dynamics Library," http://www.orocos.org/kdl.

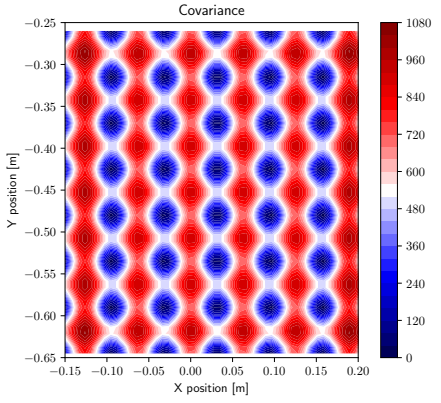

(a)

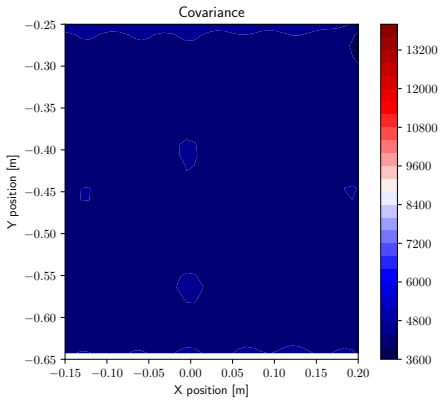

(b)

Fig. 6: Covariance functions of the $\mathcal{GP}$ model learned during the static (6a) data collection, and dynamic (6b) in-situ data collection. Blue color represent low values of covariance, while a red color indicates high values.

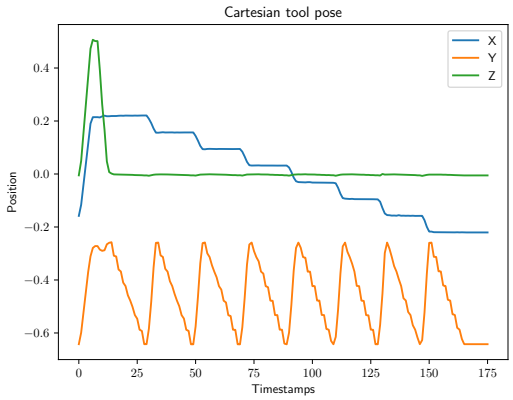

(a)

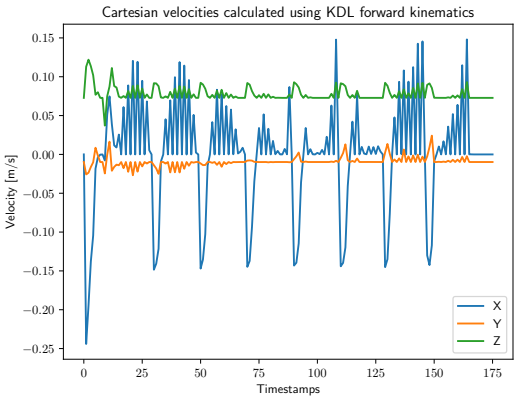

(b)

Fig. 7: Cartesian tool pose (figure 7a) and Cartesian velocities (figure 7b) in function of time during in-situ dynamic dataset collection.